

THE HIPPOCAMPUS

New Vistas

Editors

Victoria Chan-Palay

Department of Neurology
University Hospital
Zürich, Switzerland

Christer Köhler

Astra Research Center
Södertälje, Sweden

ALAN R. LISS, INC., NEW YORK

**Address all Inquiries to the Publisher
Alan R. Liss, Inc., 41 East 11th Street, New York, NY 10003.**

Copyright © 1989 Alan R. Liss, Inc.

Printed in the United States of America .

Under the conditions stated below the owner of copyright for this book hereby grants permission to users to make photocopy reproductions of any part or all of its contents for personal or internal organizational use, or for personal or internal use of specific clients. This consent is given on the condition that the copier pay the stated per-copy fee through the Copyright Clearance Center, Incorporated, 27 Congress Street, Salem, MA 01970, as listed in the most current issue of "Permissions to Photocopy" (Publisher's Fee List, distributed by CCC, Inc.), for copying beyond that permitted by sections 107 or 108 of the US Copyright Law. This consent does not extend to other kinds of copying, such as copying for general distribution, for advertising or promotional purposes, for creating new collective works, or for resale.

Library of Congress Cataloging-in-Publication Data

The Hippocampus : new vistas / editors, Victoria Chan-Palay, Christer Köhler.

p. cm. — (Neurology and neurobiology ; v. 52)

Includes bibliographies and index.

ISBN 0-8451-2756-X

1. Hippocampus (Brain)—Physiology. 2. Hippocampus (Brain)—
—Diseases. I. Chan-Palay, Victoria. II. Köhler, Christer.

III. Series.

[DNLM: 1. Hippocampus. W1 NE337B v. 52 / WL 314 H667]

QP383.25.H56 1989

599'.01'88—dc19

DNLM/DLC

for Library of Congress

89-2517
CIP

3

Ultrastructure, Development, and Plasticity of Dendritic Spine Synapses in Area CA1 of the Rat Hippocampus: Extending Our Vision With Serial Electron Microscopy and Three-Dimensional Analyses

KRISTEN M. HARRIS, FRANCES E. JENSEN, AND BEATRICE H. TSAO
Neuroscience Department, Children's Hospital, Boston, Massachusetts

INTRODUCTION

In area CA1 of the rat hippocampus, the overwhelming majority of excitatory synapses occur on protrusions from pyramidal cell dendrites referred to as "dendritic spines." Considerable attention has been focused on dendritic spines because changes in their dimensions could modulate synaptic efficacy (Chang, 1952; Rall, 1970, 1974; Harris and Stevens, 1988a; and Brown et al., 1987 for review). Complete anatomical measurements are required to interpret whether changes in spine or synaptic morphology are sufficient to mediate functional plasticity. To date, the only method available to obtain these complete measurements is three dimensional reconstructions from serial electron microscopy. In this chapter, we describe the morphology of CA1 spiny dendrites with Golgi impregnations, freeze-fracture preparations, and thin section electron microscopy. We present the rationale for studying dendritic spines through serial electron microscopy and propose some methods for overcoming the major shortcoming of serial EM—i.e. small sample sizes. Finally, we present some results that illustrate how these complete reconstructions can be used to determine whether changes in spine and synapse morphology could be involved in the ontogeny of hippocampal longterm potentiation.

CA1 Spiny Pyramidal Cell Dendrites: Qualitative Description of Spine and Synaptic Morphology

With light microscopy, it is possible to discern the tiny spines that protrude from CA1 pyramidal cell dendrites, but impossible to obtain accurate measurements of their dimensions (Fig. 1a,b). Viewed with electron microscopy, some fortunate freeze-fracture planes reveal the enormous diversity of spine morphology among near neighbors on a single dendritic shaft (Fig. 2). This diversity of spine morphology is associated with varied synaptic morphology

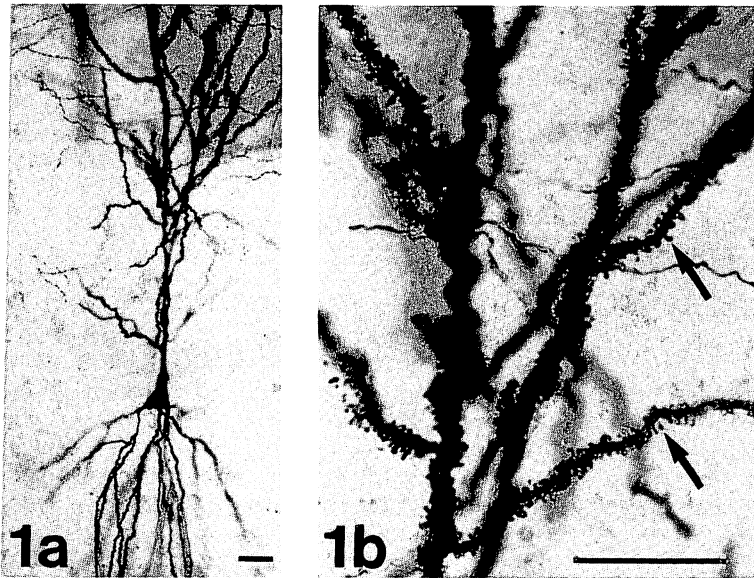
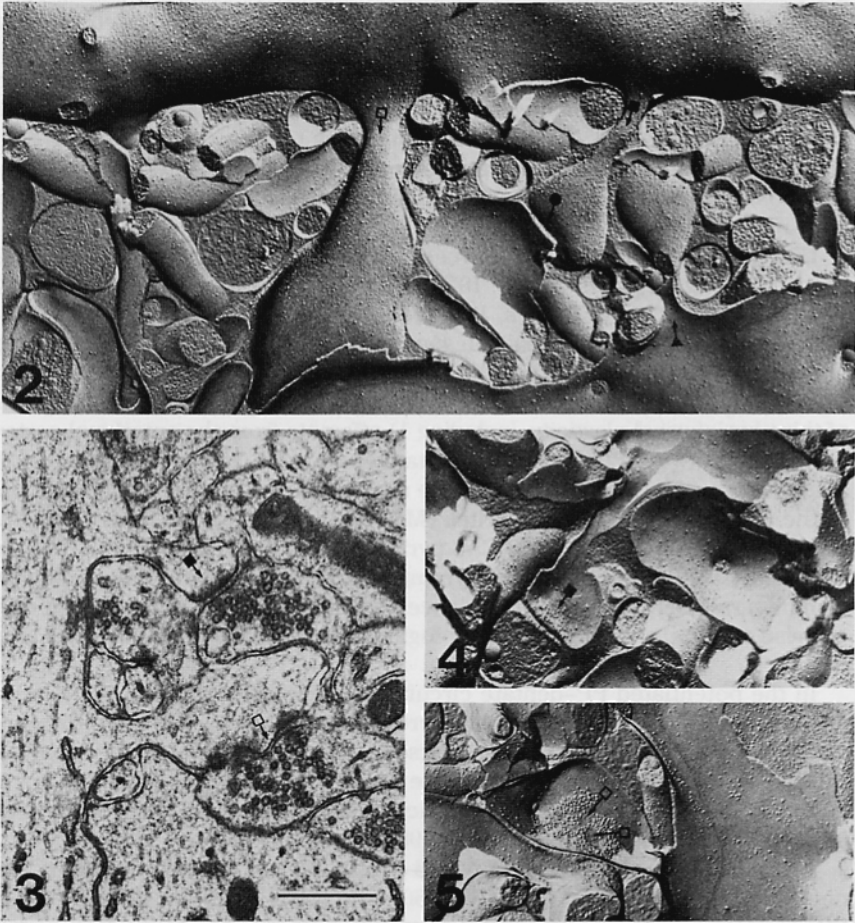


Fig. 1. **a:** A Golgi impregnation of a hippocampal CA1 pyramidal cell with apical dendrites extending up into s. radiatum. **b:** At higher magnification, dendritic spines (arrows) can be seen to stud the surface of these dendrites. Bars = 10 μ m. (Reproduced from Harris et al., 1980, with permission of the publisher.)

(Fig. 3). Spines have been qualitatively classified to have stubby, mushroom, and thin shapes (criteria for making these distinctions are described in the Results section). Small dendritic spines have asymmetric synapses with a small continuous postsynaptic density (PSD), which is macular in appearance when viewed through serial thin sections. Large mushroom-shaped dendritic spines usually have perforated asymmetric postsynaptic densities. The presynaptic axonal varicosity associated with each of these PSD morphologies contains round, clear vesicles. The organization of the particles in the fractured synaptic membrane also differs on small and large dendritic spines. The smaller, thinner spines tend to have small, continuous aggregates of particles (Fig. 4), and the larger mushroom-shaped spines have aggregates of particles that are perforated by particle-free regions (Fig. 5). While the identity of these particles is not yet known, they are associated with synapses that have characteristics of excitatory synapses, suggesting that they might be freeze-fracture representations of proteins involved in excitatory synaptic transmissions (Harris and Landis, 1986).

Plasticity of Hippocampal Spine Synapses: Single Section Analyses

Following tetanic stimulation, several afferent pathways to hippocampal cells show long-term potentiation (LTP). LTP is a long-lasting enhancement of the postsynaptic response, which can be expressed extracellularly as an



Figs. 2-5. Figure 2 shows cytoplasmic surface of a CA1 pyramidal cell dendrite revealed in profile in a freeze-fracture preparation. Very large mushroom spines (open square) are often located near smaller spines (closed square at neck, closed circle at synaptic cleft) of the same dendritic segment and on different dendritic segments (closed triangle). Figure 3 shows thin section of small dendritic spine with a macular postsynaptic density (closed square), adjacent to a large dendritic spine with a perforated postsynaptic density (open square). Figure 4 shows extracellular half of the membrane of a postsynaptic junction on a thin spine revealing a particle aggregate (closed square) at the synaptic junction. Figure 5 shows particle aggregate on the extracellular half of a larger dendritic spine with particle-free zones (open squares). Bar = 1 μ m in Figure 3 for all of Figures 2-5. (Reproduced from Harris and Landis, 1986, with permission of the publisher.)

increased field excitatory postsynaptic potential (EPSP) and population spike or intracellularly as an increased EPSP, increased probability of cell firing, or decreased latency of cell firing. The conditions for inducing LTP have been well worked out. When sufficient depolarization of the postsynaptic cells occurs in the presence of glutamate, a magnesium block is released and channels associated with the N-Methyl-D-Aspartate receptor are opened. These open channels permit a significant influx of calcium to the postsynaptic cell and thus possibly activates several second messenger-mediated events (for review, see Smith, 1987).

LTP lasts for hours, days, or weeks, depending on the exact stimulation conditions (e.g. Bliss and Lomo, 1970, 1973; Bliss and Gardner-Medwin, 1973; Alger and Teyler, 1976; Barnes, 1979). This endurance of LTP has often led to the suggestion that LTP results in some permanent or semipermanent change in synaptic number or structure (Crick, 1982; Gray, 1982). As summarized in Figure 6, four hippocampal circuits have been studied for anatomical correlates of this physiological plasticity, including 1) afferents from the entorhinal cortex, perforant pathway (PP), to area dentata granule cells (PP-dentate circuit); 2) afferents from dentate granule cells, the mossy fibers (MF), to proximal regions of the CA3 pyramidal cell dendrites (MF-CA3 circuit); 3) afferents from the septum to distal regions of the CA3 pyramidal cell dendrites (septal-CA3 circuit); and 4) afferents from CA3 pyramidal cells, the Schaffer collaterals and commissural fibers, to CA1 pyramidal cell dendrites (CA3-CA1 circuit). In each of these circuits, a variety of morphological changes have been observed after LTP.

In the potentiated PP-dentate circuit, the spine heads appear to be larger and the spine necks shorter (van Harrevel and Fifkova, 1975; Fifkova and Van Harrevel, 1977; Fifkova and Anderson, 1981; Fifkova et al., 1982). Analyses of the PSD suggest an increase in size and a shift in shape from convex to concave; and the number of presynaptic vesicles adjacent to the synaptic cleft increases (Desmond and Levy, 1983, 1986a,b, 1987).

Analyses of the potentiated MF-CA3 circuit suggest that spines swell, spine necks widen (Moshkov et al., 1977, 1980), and PSDs lengthen, similarly to the PP-dentate circuit (Petukov and Popov, 1986). In contrast to the PP-dentate circuit, vesicle number has been observed to decrease following LTP in parallel with an increase in Smooth Endoplasmic Reticulum (SER) in the axonal varicosity (Petukov and Popov, 1986).

Like the PP-dentate and MF-CA3 circuits, results from the potentiated septal-CA3 circuit suggest spine swelling, though there are no data on the neck dimensions. In contrast to the PP-dentate circuit, the potentiated septal-CA3 circuit appears to have a decrease in both length and thickness of the PSD and a decrease in the number of presynaptic vesicles (Wenzel et al., 1985).

The CA3-CA1 circuit contrasts with all three of the other circuits in that no overt spine swelling or neck widening has been observed with potentiation, though a decrease in the variability of spine perimeters has been interpreted to result from spine "rounding" (Lee et al., 1980; Chang and Greenough, 1984).

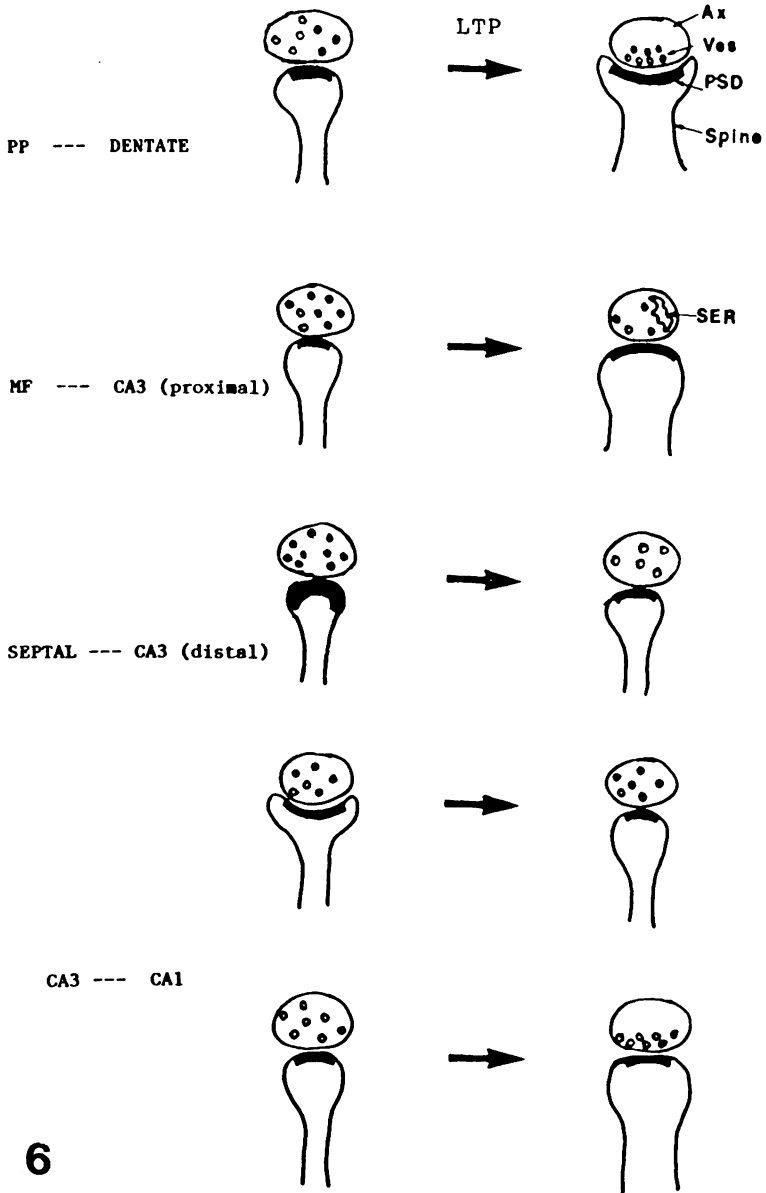


Fig. 6. Changes in spine and synaptic morphologies that have been associated with hippocampal long-term potentiation. See text for description and terminology.

Other studies suggest that spine swelling might occur in the potentiated CA3-CA1 circuit (Applegate et al., 1987). In contrast to the PP-dentate circuit, results from these studies in area CA1 suggest a decrease in PSD length and an interconversion of the PSD shape from concave to convex (Chang and Greenough, 1984). One report suggests no change in vesicle number (Chang and Greenough, 1984), while another suggests that vesicles migrate, producing a higher density at the synaptic cleft in the potentiated CA3-CA1 circuit (Applegate et al., 1987).

All of these results strongly suggest that dramatic changes in spine and synaptic morphology can be associated with hippocampal long-term potentiation. The opposite changes in spine and synaptic morphology that appear to occur in different circuits might be related to differences in receptor types, second-messenger systems, tissue preparation, or other factors.

Several questions remain. How large are the actual anatomical changes in spine or synapse morphology? Are existing synapses growing and changing their shapes, or are new synapses forming to support LTP? Are changes occurring only in a subpopulation of stimulated spines and synapses, or do all the affected spines and synapses show the same shifts in their morphology? Are the changes in spine morphology sufficient to modify the transfer of charge from the synapse through the spine neck to the parent dendrite?

To answer these questions, complete descriptions of spine and synaptic morphologies are required. A serial section analysis allows for a complete description of each spine and its associated synapse, including 1) measurement of the whole spine and synapse, 2) unambiguous identification of each structural element, and 3) three-dimensional reconstructions for quantitative shape analyses. This approach has several advantages over the random-section analyses that have been used thus far to observe changes in dendritic spines and synapses. Relationships between changes in the shape of individual spines and their synapses can be easily discerned. Accurate measurements of individual spine characteristics, such as head diameter, neck diameter, and neck length, can be used to model charge transfer through spines and discern whether measured anatomical changes are sufficient to modify charge transfer (e.g. Wilson et al., 1983; Wilson, 1984; Harris and Stevens, 1988b, 1989). Spine neck and head volumes can be measured and used in theoretical models to determine how changes in shape might alter diffusion properties in the dendritic spine (e.g. Shepherd, 1979; Gamble and Koch, 1987; Brown et al., 1977; Harris and Stevens, 1988b, 1989).

These advantages might be tempered by the time required to obtain a large sample of complete reconstructions from dendritic spines and synapses. However, this must be weighed against the strong advantage of having accurate measurements and identity. Fewer total numbers need be analyzed to reveal dramatic differences in morphology. We present here a strategy we have used to optimize these advantages for analysis of developing hippocampal dendritic spines (Harris et al., 1987; Harris et al., manuscript in preparation) and the possible relationship of developmental changes in their shapes to the ontogeny of LTP (Harris and Teyler, 1984).

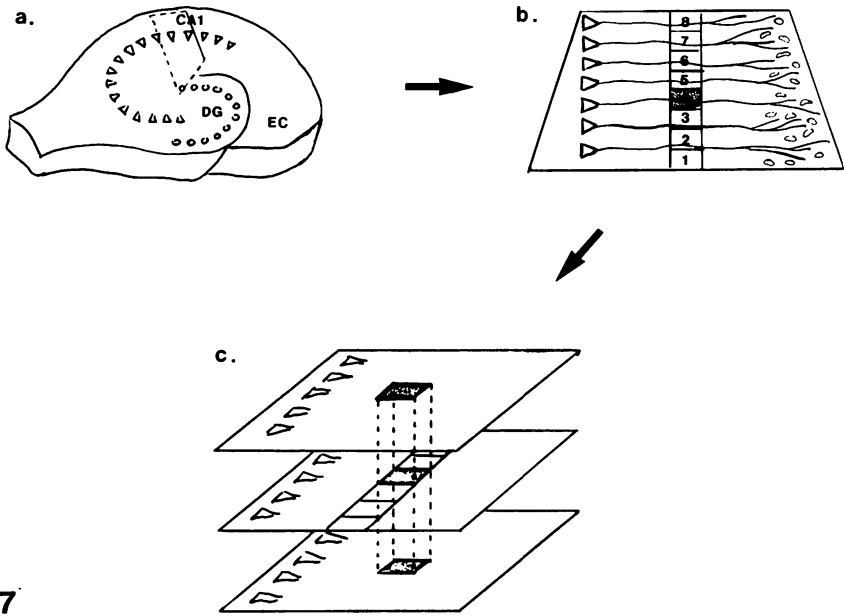
DEVELOPMENT AND PLASTICITY OF HIPPOCAMPAL SPINE SYNAPSES: SERIAL EM ANALYSES

Detailed methods for tissue preparation and serial electron microscopy have been described elsewhere (Stevens et al., 1980; Stevens, 1980; Stevens and Trogadis, 1984; Harris and Landis, 1986; Harris and Stevens, 1988a,b). Here we will describe procedures that have been developed to sample the neuropil to obtain good estimates of the frequency of different spine and synaptic morphologies and accurate measurements of synaptic areas.

To locate sample fields, the photographic screen of the electron microscope was calibrated at the desired magnification (usually 6.6 K on a JEOL 100B) with a calibration grid. Then the calibrated screen was used to measure a distance from the pyramidal cell body layer out to 250 μm in stratum radiatum. This procedure requires a rotation stage so that one can move perpendicularly from the pyramidal cell layer into s. radiatum. Using the calibrated screen, a strip located in s. radiatum measuring about 25 μm wide and running perpendicular to the pyramidal cell bodies was divided into eight to ten equal fields, each about 500 μm^2 (Fig. 7). A random number table was consulted to determine which of these fields to photograph through adjacent serial sections. The "sample" field of 200 μm^2 is located on the middle section of the series. The reason for making the sample field smaller than the photographic field is to allow for slight shifts in the alignment from section to section, which could result in loss of sample structures at the edge of the micrograph if all 500 μm^2 were sampled.

Adjacent sample fields in s. radiatum often have very different structural components occupying the neuropil. In Figure 8, the neuropil is filled with small dendrites, spine heads, and axons. Most of this neuropil contains structures that are part of the synaptic complex. In contrast, large, longitudinally sectioned dendrites fill much of the neuropil of the field in Figure 9. It is impossible for synapses to form in the central cytoplasm of these dendrites; therefore, the sample areas of these two adjacent fields are not equivalent for calculating synaptic densities.

A method was devised to determine which processes should be subtracted from the total sample area to give a corrected sample area with homogeneity of variance among the size of dendritic processes in it. Five randomly selected fields, including these two fields, were photographed. If a blood vessel was in the field, the photographic screen was moved laterally to exclude the vessel. Then the enclosed area of every dendritic process in the field was measured. Spines, unmyelinated axons, and axonal varicosities are smaller than these processes and were excluded from this analysis. The frequencies of dendritic process areas for each field are plotted in Figure 10. The mean process area and variance were computed for each field (Table I, "before correction"). Then the two fields with the most disparate variance (Nos. 2 and 5) were compared for homogeneity of variance among dendritic process areas. All process areas greater than 2 μm^2 were excluded from the sample to achieve homogeneity of variance across the five fields (Table I, "after correction"). The corrected

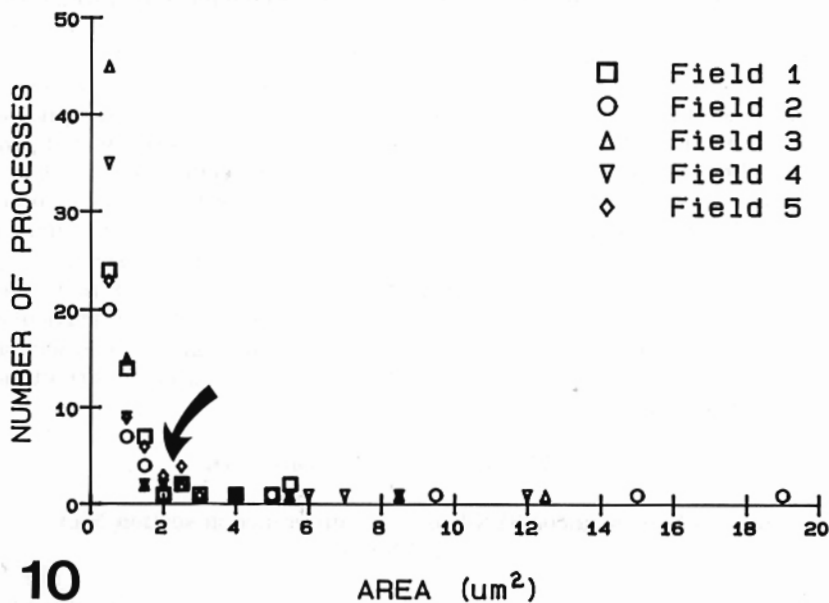
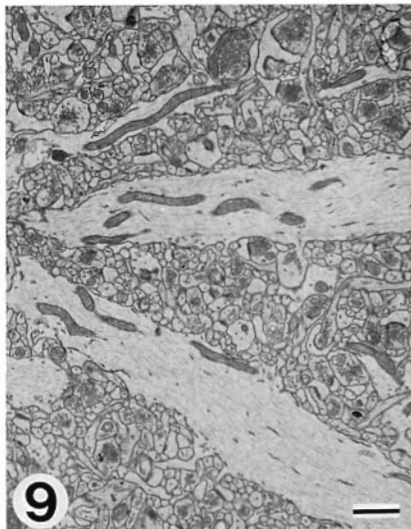
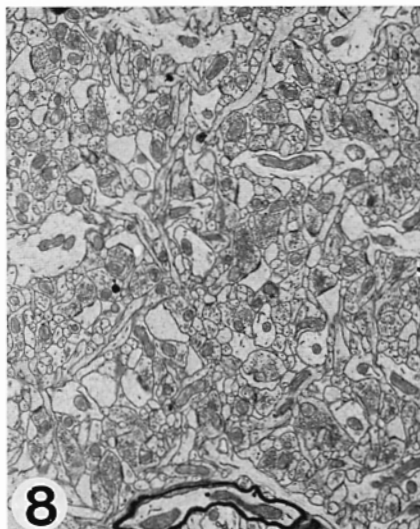


7
 Fig. 7. Sample field selection in stratum radiatum of hippocampal area CA1 (DG-dentate gyrus; EC-entorhinal cortex). **a:** The trapezoid is trimmed to contain the CA1 pyramidal cell bodies and the entire apical dendritic field (full length approximately equalling 0.8 mm). **b:** A sample field located about 250 μm from the outer edge of the pyramidal cell layer is randomly selected from the eight to ten possible fields across the width of the section (approx. 0.2 mm). **c:** The sample field is then photographed through 40 adjacent serial thin sections.

neuropil area (NA) = Total sample area - (glia area - myelinated axon area - dendritic cytoplasm of processes $> 2 \mu\text{m}^2$).

Every synapse with a portion located on the sample field of the central section was completely reconstructed through adjacent serial sections. For cross-sectioned synapses, the area of the PSD was determined by measuring its length through adjacent sections, multiplying the lengths by section thickness, and then adding across sections. Section thickness was determined empirically as described by Harris and Stevens (1988a,b). For obliquely or tangentially sectioned PSDs, the enclosed area was measured on each section on which it appeared.

Figs. 8, 9. Adjacent sample fields within s. radiatum. These figures contain about 50 μm^2 of the sample fields. They illustrate the extreme inhomogeneity in structural composition of the neuropil where small dendritic processes fill Figure 8 and large dendritic processes occupy much of the field in Figure 9. Bar = 1 μm .



10
 Fig. 10. Dendritic processes with measured cross-sectional areas on the sample fields. To obtain homogeneity of variance in process sectioned areas across these five fields, all processes with areas greater than $2 \mu\text{m}^2$ (curved arrow) were excluded from the sample area. See also Table I.

TABLE I. Effect of Excluding Large Dendritic Processes From Sample Fields on the Mean and Variance of the Process Areas Occupying These Fields*

| Field | n | Before correction | | n' | After correction | |
|-------|----|-------------------|----------|----|------------------|----------|
| | | Mean | Variance | | Mean | Variance |
| 1 | 53 | 0.98 | 1.60 | 46 | 0.57 | 0.47 |
| 2 | 38 | 1.80 | 15.76 | 32 | 0.51 | 0.46 |
| 3 | 69 | 0.80 | 3.38 | 64 | 0.39 | 0.38 |
| 4 | 54 | 1.15 | 5.06 | 48 | 0.43 | 0.40 |
| 5 | 47 | 0.83 | 0.71 | 41 | 0.57 | 0.48 |

*Mean is expressed as μm^2 ; n is number of processes measured in each field, and n' is number of processes remaining after excluding those with areas $>2.0 \mu\text{m}^2$.

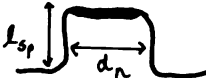

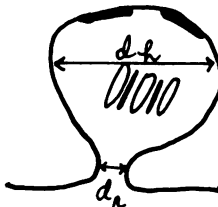
We recognized that the probability of observing part of a synapse on the sample field was proportional to the number of sections that the synapse actually occupied through serial sections. If a synaptic type changed size, shape, or orientation to change significantly the probability of viewing them on the sample field, then the number of sections on which they appeared would change proportionately. For example, if an elliptical synapse was sectioned at $0.07 \mu\text{m}$ thickness, perpendicular to a short axis with a diameter of $0.21 \mu\text{m}$, three sections of the synapse would be obtained. In a nine-section series, with random placement of this synapse in the series, the probability of viewing the synapse on any one of the nine sections is $3/9$ or $1/3$. If the same synapse were sectioned parallel to a long axis with a diameter of $0.42 \mu\text{m}$, six sections of the synapse would be obtained. Random placement in the nine-section series would give a probability of viewing the same synapse in any one section of $6/9$ or $2/3$ —a 100% increase in the probability of viewing that synapse on the sample section.

For each synapse appearing on the sample section, we counted the number of serial sections on which it appeared. Then, when grouping the synapses by type, we computed the average number of sections for each type. If there was a significant difference in the number of sections occupied by a particular synaptic type that occur at one age from another, then the %difference in section number was calculated. Then the following formulae were used to correct the relative synaptic densities (corrSYNDens):

$$\text{uncorrSYNDens} = \text{No. of synapses/NA}$$

$$\text{corrSYNDens} = \text{uncorrSYNDens} - [(\% \text{difference in section No.}) \cdot (\text{uncorrSYNDens})]$$

The postsynaptic element associated with each synapse was identified by viewing it through adjacent serial sections. Dendritic spines were first classified into three shape categories of stubby, mushroom, and thin according to the criteria listed in Figure 11. Then a randomly selected subpopulation of these spines was reconstructed to confirm the shape assignments. The reconstruc-

| <u>CLASS</u> | <u>SHAPE</u> | <u>CRITERIA</u> |
|--------------|---|------------------------------------|
| stubby |  | $d_n \geq l_{sp}$ |
| thin |  | $d_n \ll l_{sp}$ $d_n \leq d_h$ |
| mushroom |  | $d_n \ll d_h$ |

11

Fig. 11. Classification of dendritic spines by shape as viewed through serial thin sections. The criterion for a stubby dendritic spine was that the diameter of the neck (d_n) be greater than or equal to the spine length (l_{sp}). The criteria for a thin spine were that the neck diameter be much less than the total length and that the diameter of the head (d_h) be not much greater than the neck diameter. A spine was classified as a mushroom shape if the diameter of the neck was very much less than the head diameter. These mushroom spines frequently had perforated synapses and well-developed spine apparatuses in adult hippocampus.

tions were obtained using a reconstruction system that includes a Gould Image Processing System interfaced to a VAX 780 and a Cohu monochromatic camera mounted on a copy stand. Electron micrographs were positioned under the video camera, images captured with the Gould system, and traces superimposed on the EM image viewed on the Gould monitor. Quantitative analyses of the reconstructions were obtained with the PANDORA software (Pearlstein et al., 1986).

RESULTS

Development of Synapses in Stratum Radiatum: Sample Field Analyses

We have used the methods described above to evaluate synaptic morphology in the developing hippocampus at three postnatal ages: P7, P15, and adult. These ages were chosen because it was shown in an earlier study that the ontogeny of LTP begins postnatally in hippocampal area CA1 (Harris and Teyler, 1984). Before P5, tetanic stimulation (100 Hz for 1 s) does not induce long-lasting changes in the population response; by P5, half of the animals showed potentiation of the population spike amplitude; and by P7 all of the animals

showed robust LTP. At P15, the magnitude of LTP was three times greater than that observed in adult animals (see Fig. 3 in Harris and Teyler, 1984). Our preliminary anatomical analyses reveal striking differences in the frequencies of the different classes of synaptic and spine morphologies across these ages (a detailed description and quantitative analysis is being prepared by Harris et al.).

Thus far, 232 synaptic PSD areas have been measured through complete reconstructions. Five categories of postsynaptic elements were identified with these synapses by viewing them through serial thin sections, including unclassified, shaft, stubby spine, mushroom spine, or thin spine.

At P7 (LTP onset), four sample fields (100–150 μm^2 each) were analyzed. In these fields, seven synapses could not be unambiguously identified by class. These unclassified P7 synapses were of the same average area as synapses occurring on dendritic shafts ($N = 18$), stubby spines ($N = 5$), and a mushroom spine ($N = 1$; Fig. 12). There are no postsynaptic elements that could be identified as thin spines at P7.

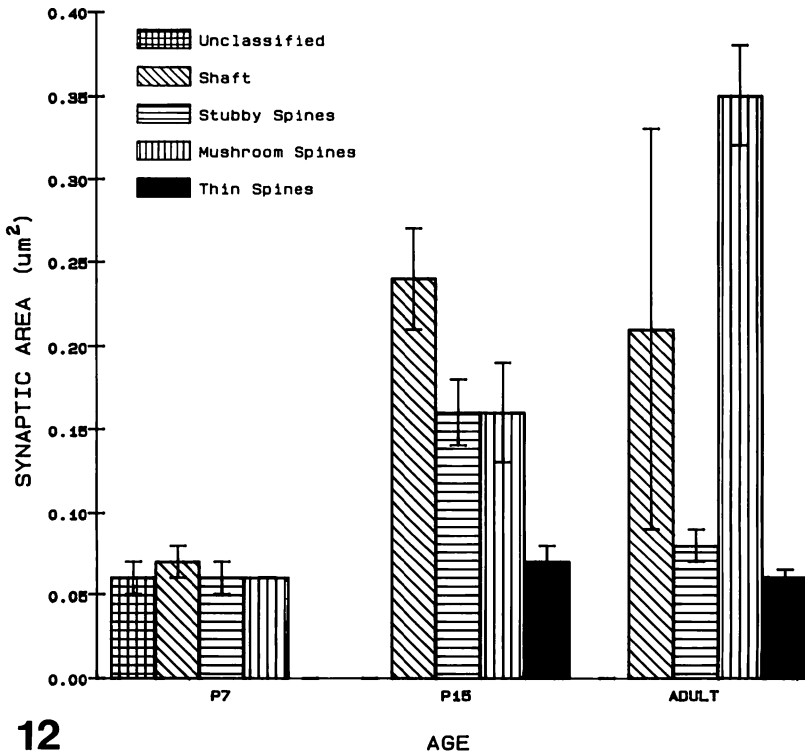


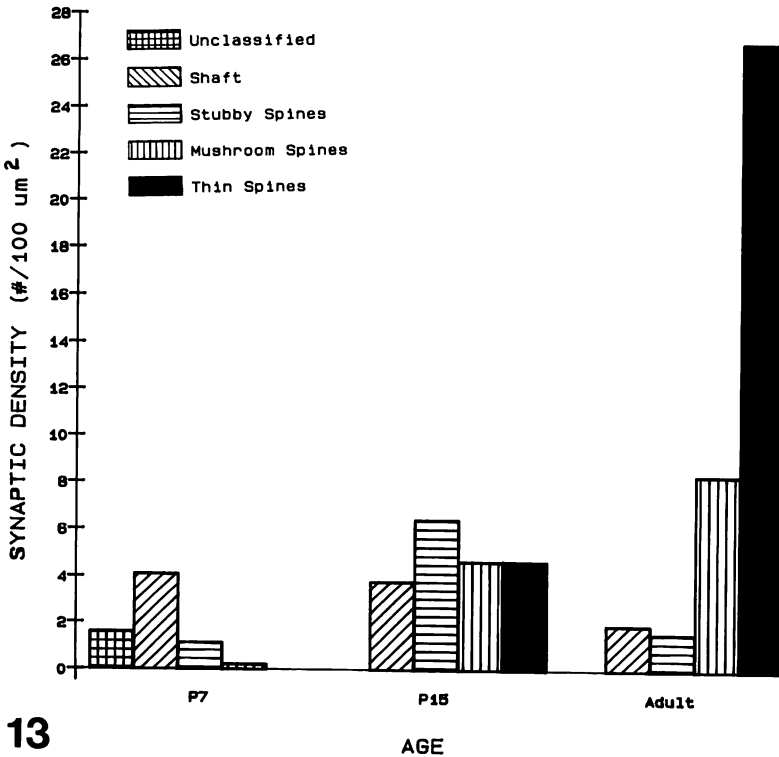
Fig. 12. Synaptic area, measured through serial sections, at different classes of postsynaptic structures (mean \pm S.E.M.) at postnatal days 7 (P7), 15 (P15), and adult.

Three-Dimensional Analysis of CA1 Dendritic Spines / 45

At P15 (LTP peak), two sample fields ($NA = 171.06$ and $183.76 \mu\text{m}^2$) were analyzed. All of the postsynaptic elements were readily identified, and all classes of synapses (shaft, $N = 13$; stubby, $N = 21$; mushroom, $N = 15$; and thin, $N = 16$) were larger than at P7, suggesting growth in synaptic area between these two ages (Fig. 12).

In the adult (LTP decline), analysis of two sample fields ($NA = 128.5$ and $170.64 \mu\text{m}^2$) revealed no further significant increase in the size of synapses on dendritic shafts ($N = 5$). The size of synapses of stubby spines ($N = 5$) decreased significantly from the P15 value ($P < 0.003$). The size of synapses on mushroom spines ($N = 44$) increased significantly from the P15 value ($P < 0.0001$). The slight decrease in average synaptic area on thin spines from the P15 to the adult value ($N = 87$) was not significant (Fig. 12).

The relative densities of these different synaptic classes were computed from each of these sample fields, and the mean values are presented in Figure 13. To obtain an estimate of synaptic densities in each class at each age we first computed the number of synapses per corrected neuropil area as described



13
Fig. 13. Density of different classes of postsynaptic structures at each age.

above. We used P15 as the age of comparison for %difference in section number to correct further the relative synaptic densities (as described above for corrSYNdens). Only the mushroom spines showed a significant difference in the number of sections their synaptic PSD occupied, which increased between P15 and P60.

At P7, most synapses were associated with unclassified dendritic shafts or with stubby dendritic spines. Occasionally a mushroom spine was observed. At P15, synapses were distributed relatively evenly between all four classes of postsynaptic elements. In the adult, many fewer shaft and stubby spines are present than at P15. The density of mushroom spines doubles, even when corrected for the increase in the probability of observing them on the sample field because of the significant increase in PSD area. There is a dramatic fourfold increase in the density of synapses located on thin dendritic spines between P15 and adulthood.

Development of Spine Morphology: Three-Dimensional Reconstructions To Confirm Visual Identity

Two P15, stubby dendritic spines are illustrated in Figure 14. These stubby spines had large, well-developed synaptic complexes, complete with a thickened PSD, a widened cleft, and a presynaptic axonal varicosity filled with round, clear vesicles. This spine morphology was rare in the adults, in which thin spines prevailed. To test spine classification as identified by viewing them through serial sections, 12 dendritic spines (two in each spine class from the sample fields at P15 and adult) have been completely reconstructed. Six of these spines are illustrated in Figure 15. Of these 12 spines, 11 were correctly identified. One P15 mushroom spine was misidentified as a thin spine. It had a relatively small head for the mushroom category, but the head diameter was clearly larger than the neck diameter when completely reconstructed. More of these reconstructions are being completed to be tested in biophysical models of charge transfer through the necks and to discern whether they occur in quantitatively discrete shape categories at each age or if there are perhaps more "transitional" shapes at younger ages (e.g. shapes that are halfway between stubby and mushroom or between mushroom and thin).

DISCUSSION: PROPOSED SEQUENCE OF SPINE DEVELOPMENT IN HIPPOCAMPAL AREA CA1—IMPLICATIONS FOR THE ONTOGENY OF LTP

A sequence for spine development in area CA1 is proposed in Figure 16. These anatomical observations would be consistent with the view that hippocampal stubby spines develop from shaft synapses, because more shaft than spine synapses are present at P7. The stubby spine might be a precursor of mushroom spines or of long, thin spines, because more stubby spines are present at P15 than in the adult. It is unlikely that long, thin spines form first and then contract to become stubby spines, because many stubby spines are present at P7 and P15 while very few stubby spines are present in the adult. Alternatively, thin spines might be remodeled from mushroom spines. This second

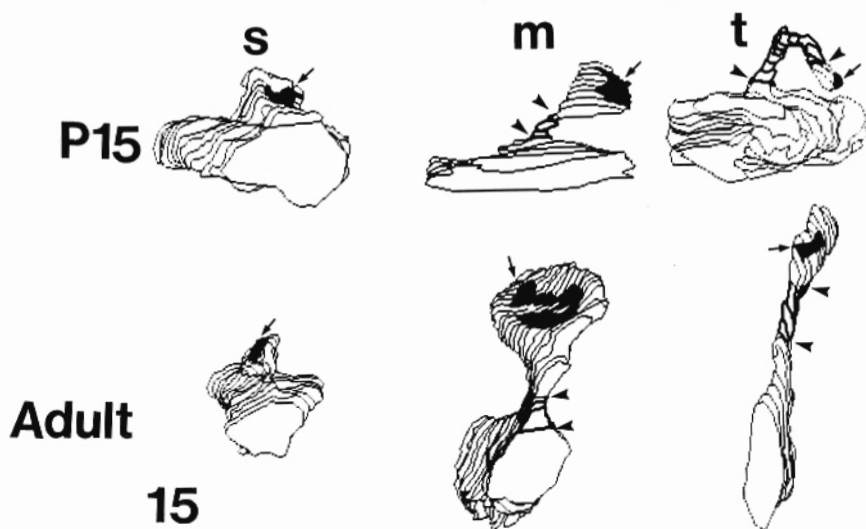
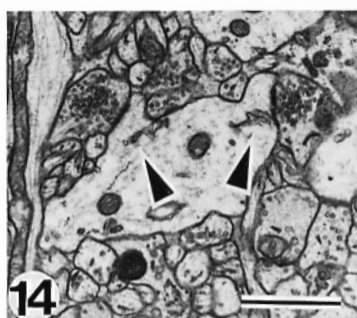


Fig. 14. Two stubby dendritic spines (arrow heads) from P15 hippocampal area CA1. Bar = 1 μ m for Figures 14 and 15.

Fig. 15. Three-dimensional reconstructions of dendritic spines at P15 and adult ages to illustrate spine shape categories of stubby (s), mushroom (m), and thin (t). Synaptic areas (arrows) are filled in on the spine heads (thin lines). Spine necks are divided from spine heads for mushroom and thin spines (bold lines between arrowheads). A portion of the dendritic shaft that each spine was connected to is also illustrated. See Figure 14 for scale bar.

view is supported by the relative abundance of stubby and mushroom spines and the relative absence of thin spines at P7 and P15, suggesting that the stubby and mushroom shapes might precede the thin spine shape. Analyses are in progress to determine whether stubby, mushroom, and thin spines occur in discrete categories with quantitative distinctions separating them (e.g. the ratio of head volume to neck diameter) or represent a continuum in shape dimensions across development.

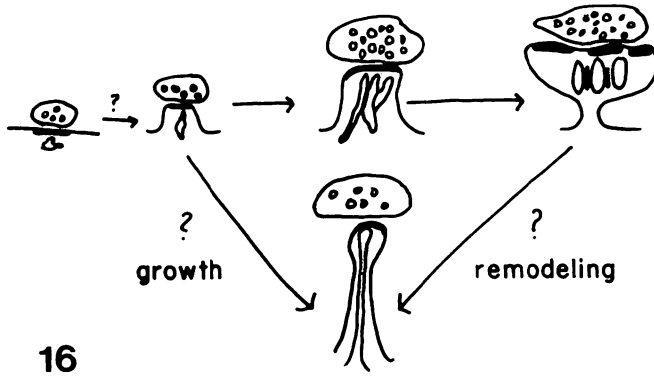


Fig. 16. Proposed sequence of spine development that is consistent with the preliminary anatomical findings reported here.

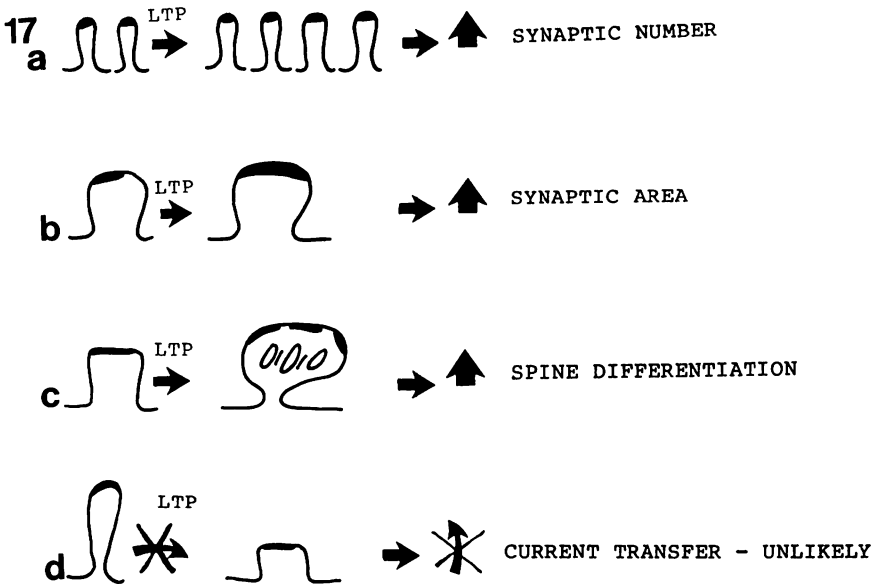


Fig. 17. Possibilities for changes in spine or synaptic morphology of hippocampal CA1 pyramidal cells that could be associated with LTP at ages P7 and P15. See text for further description.

Since more synapses are present in adult animals than at P15, the peak and decline in LTP around P15 is not directly related to the absolute number of synapses present. Our hypothesis has been that a larger percentage of synapses can produce LTP at P15 than in adult animals (Harris and Teyler, 1984). We proposed that synapses are removed from a pool of "plastic" synapses as they are "used" to process experiences, thus explaining how a peak and decline in LTP production might be related to synaptogenesis (see Fig. 11 in Harris and Teyler, 1984).

The anatomical observations presented here suggest several changes in spine and synaptic morphology that could occur with LTP at P15 (Fig. 17). At P15, tetanic stimulation could induce more synapses (e.g. more thin spines with synapses) to form (Fig. 17a). Synaptic area could grow to produce LTP and might do so at a greater extent during robust synaptogenesis (P15) than in adults (Fig. 17b). Undifferentiated stubby or mushroom spines might be induced to undergo a change in P15 hippocampus more readily than in adult hippocampus (Fig. 17c).

It seems *unlikely* that the peak in LTP magnitude is mediated by a large population of long, thin spines, which shorten and widen to facilitate charge transfer to the parent dendrite (Fig. 17d). If this were so, we would expect the magnitude of LTP observed in adult animals to be larger than at P15, because many more thin spines are available for "contraction" in the adult than at P15. In addition, it seems unlikely that long, thin spines are necessary for LTP induction, because few, if any, are present at P7, an age when LTP is robust.

It could be that spine differentiation from stubby to mushroom or thin spines with constricted spine necks facilitates partitioning of synapses onto relatively isolated compartments, i.e. the spine head (Harris and Stevens, 1988b, 1989). This partitioning of dendritic spines could prevent diffusion of second messengers, phosphorylated proteins, or other postsynaptic products of LTP away from the activated synapses, thereby restricting LTP to those synapses that are potentiated. This restriction might serve to prevent heterosynaptic potentiation. The relative absence of constricted spine necks at P15 might result in nonspecific heterosynaptic potentiation, leading to a larger response magnitude because neighboring "unpotentiated" synapses were also "potentiated" by diffusing substances (see Harris and Stevens, 1988b, 1989; Brown et al., 1987). If this were so, the peak in LTP magnitude observed at P15 could be an immaturity of response specificity, a possibility that will be tested physiologically in subsequent experiments. In conjunction with the serial EM approach described here, it should be possible to discern whether changes in spine shape are sufficient to contribute to the peak and decline in LTP magnitude observed during development.

SUMMARY

The goal of this chapter was to illustrate our strategy for optimizing the use of complete reconstructions from serial EM to obtain accurate measurement and identification of dendritic spines and their associated synapses. We have observed a dramatic shift from stubby and mushroom-shaped dendritic

spines at P7 (LTP onset) and P15 (LTP peak) to a predominance of long, thin spines in adult (LTP decline) hippocampal area CA1. We propose a sequence for the genesis of dendritic spines from short stubby protrusions to either mushroom-shaped spines or long, thin spines. Hypotheses concerning the role(s) of dendritic spines in the ontogeny of hippocampal LTP were considered in light of these preliminary anatomical findings.

ACKNOWLEDGMENTS

We thank Gene Zilberstein and Nariman Shambayati of the Image Graphics Laboratory at Children's Hospital for implementing software used for the reconstructions, editing, and displays in these studies. We thank Dr. John Stevens and Judy Trogadis of the University of Toronto for teaching K.M.H. many of the principles of serial EM and for use of their reconstruction system during earlier phases of this work; Dr. D. Max Snodderly and Dr. Thomas Brown for helpful discussions of the results; and Greg Belmont and Dr. Robert Baughman for improving an earlier version of this manuscript. This work is supported by NIH-NINCDS grant NS21184 and The Alfred P. Sloan Foundation (K.M.H.), NIH-NICHD grant HD00807 (F.E.J.), a Radcliffe Summer Project Grant (B.H.T.), NIH grant NS20820 (R.L. Sidman, P.I.), and MRC grants MT-7345 and MA-8304 (J.K. Stevens, P.I.).

REFERENCES

- Alger, B.E., and T.J. Teyler (1976) Long-term and short-term plasticity in CA1, CA3, and dentate regions of rat hippocampal slice. *Brain Res.* 110:463-480.
- Applegate, M.D., D.S. Kerr, and P. Landfield (1987) Redistribution of synaptic vesicles during hippocampal long term potentiation. *Brain Res.* 401:401-406.
- Barnes, C.A. (1979) Memory deficits associated with senescence: A neurophysiological and behavioral study in the rat. *J. Comp. Physiol. Psychol.* 93:74-104.
- Bliss, T.V.P., and A.R. Gardner-Medwin (1973) Long-lasting potentiation of synaptic transmission in the dentate area of the unanaesthetized rabbit following stimulation of the perforant path. *J. Physiol.* 232:357-374.
- Bliss, T.V.P., and T. Lomo (1970) Plasticity in a monosynaptic cortical pathway. *J. Physiol.* 207:61P.
- Bliss, T.V.P., and T. Lomo (1973) Long-lasting potentiation of synaptic transmission in the dentate area of the anaesthetized rabbit following stimulation of the perforant path. *J. Physiol.* 232:331-356.
- Brown, T.H., V.C. Chang, A.H. Ganong, C.L. Keenan, and S.R. Kelso (1987) Biophysical properties of dendrites and spines that may control the induction and expression of long-term synaptic potentiation. In P.W. Landfield and S.A. Deadwyler (eds): *Long-Term Potentiation: From Biophysics to Behavior*. New York: Alan R. Liss, Inc., pp. 201-264.
- Chang, H.T. (1952) Cortical neurons with particular reference to the apical dendrites. *Cold Spring Harbor Symp. Quant. Biol.* 17:189-202.
- Chang, F.L.F., and W.T. Greenough (1984) Transient and enduring morphological correlates of synaptic activity and efficacy in the rat hippocampal slice. *Brain Res.* 309:35-46.
- Crick, F. (1982) Do dendritic spines twitch? *Trends Neurosci.* 5:44-46.

Three-Dimensional Analysis of CA1 Dendritic Spines / 51

- Desmond, N.L., and W.B. Levy (1983) Synaptic correlates of associative potentiation/depression: An ultrastructural study in the hippocampus. *Brain Res.* 265:21-30.
- Desmond, N.L., and W.B. Levy (1986a) Changes in the numerical density of synaptic contacts with long-term potentiation in the hippocampal dentate gyrus. *J. Comp. Neurol.* 253:466-475.
- Desmond, N.L., and W.B. Levy (1986b) Changes in the postsynaptic density with long-term potentiation in the dentate gyrus. *J. Comp. Neurol.* 253:476-482.
- Desmond, N.L., and W.B. Levy (1987) Anatomy of associative long-term synaptic modification. In P.W. Landfield and S.A. Deadwyler (eds): *Long-Term Potentiation: From Biophysics to Behavior*. New York: Alan R. Liss, pp. 265-305.
- Fifkova, E., and C.L. Anderson (1981) Stimulation-induced changes in dimensions of stalks of dendritic spines in the dentate molecular layer. *Exp. Neurol.* 74:621-627.
- Fifkova, E., C.L. Anderson, S.J. Young, and A. van Harrevelde (1982) Effect of anisomyosin on stimulation-induced changes in dendritic spines of the dentate granule cells. *J. Neurocytol.* 11:183-210.
- Fifkova, E. and A. Van Harrevelde (1977) Long-lasting morphological changes in dendritic spines of dentate granular cells following stimulation of the entorhinal area. *J. Neurocytol.* 6:211-230.
- Gamble, E., and C. Koch (1987) The dynamics of free calcium in dendritic spines in response to repetitive synaptic input. *Science* 236:1311-1315.
- Gray, E.G. (1982) Rehabilitating the dendritic spine. *Trends Neurosci.* 5:5-6.
- Harris, K.M., W.L.R. Cruce, W.T. Greenough, and T.J. Teyler (1980) A Golgi impregnation technique for thin brain slices maintained in vitro. *J. Neurosci. Methods* 2:363-371.
- Harris, K.M., F.E. Jensen, and B. Tsao (1987) Development of hippocampal LTP, synapses, and spines. *Soc. Neurosci. Abs. Vol. 13*:394.12.
- Harris, K.M., and D.M.D. Landis (1986) Synaptic membrane structure in area CA1 of the rat hippocampus. *Neuroscience* 19:857-872.
- Harris, K.M., and J.K. Stevens (1988a) Study of dendritic spines by serial electron microscopy and three-dimensional reconstructions. In R.J. Lasek and M.M. Black (eds): *Intrinsic Determinants of Neuronal Form and Function*. New York: Alan R. Liss, pp. 179-199.
- Harris, K.M., and J.K. Stevens (1988b) Dendritic spines of rat cerebellar Purkinje cells: Serial electron microscopy with reference to their biophysical characteristics. *J. Neurosci.* 8:4455-4469.
- Harris, K.M. and J.K. Stevens, (1989) Dendritic spines of CA1 pyramidal cells in the rat hippocampus: Serial electron microscopy with reference to their biophysical characteristics. *J. Neurosci.* (in press).
- Harris, K.M., and T.J. Teyler (1984) Developmental onset of long-term potentiation in area CA1 of the rat hippocampus. *J. Physiol.* 346:27-48.
- Lee, K.S., F. Schottler, M. Oliver, and G. Lynch (1980) Brief bursts of high-frequency stimulation produce two types of structural change in the rat hippocampus. *J. Neurophysiol.* 44:247-258.
- Moshkov, D.A., L.L. Petrovskaia, and A.G. Bragin (1977) Posttetanic changes in the ultrastructure of the giant spicous synapses in hippocampal field CA3. *Dokl. Akad. Nauk. USSR* 237:1525-1528.
- Moshkov, D.A., L.L. Petrovskaia, and A.G. Bragin (1980) Ultrastructural study of the bases of postsynaptic potentiation in hippocampal sections by the freeze-substitution method. *Tsitologija* 22:20-26.

- Pearlstein, R.A., L. Kirschner, J. Simons, S. Machell, W.F. White, and R.L. Sidman, (1986) A multimodel system for reconstruction and quantification of neurologic structures. *Anal. Quant. Cytol. Histol.* 8:108-115.
- Petukhov, V.V., and V.I. Popov (1986) Quantitative analysis of ultrastructural changes in synapses of the rat hippocampal field CA3 in vitro in different functional states. *Neuroscience* 18(4):823-835.
- Rall, W. (1970) Cable properties of dendrites and effects of synaptic location. In P. Andersen and J.K.S. Jensen (eds): *Excitatory Synaptic Mechanisms*. Proceedings of the 5th International Meeting of Neurobiologists. Oslo: Universitets Forlaget, pp. 175-187.
- Rall, W. (1974) Dendritic spines, synaptic potency and neuronal plasticity. In C. Woody, K. Brown, T. Crow, and J. Knispel (eds): *Cellular Mechanisms Subservicing Changes in Neuronal Activity*. Los Angeles, CA: Brain Information Service, UCLA.
- Shepherd, G.M. (1979) *The Synaptic Organization of the Brain*. New York: Oxford University Press, p. 364.
- Smith, S.J. (1987) Progress in LTP at hippocampal synapses—A post synaptic Ca^{2+} trigger for memory storage. *Trends Neurosci.* 10:142-144.
- Stevens, J.K. (1980) Reconstructing neuronal microcircuitry: Using computers to assemble three dimensional structures from montages of serial electron microscopy. *Bull. Micro. Soc. Can* 8:4-12.
- Stevens, J.K., T. Davis, N. Friedman, and P. Sterling (1980) A systematic approach to reconstructing microcircuitry by electron microscopy of serial sections. *Brain Res. Rev.* 2:265-293.
- Stevens, J.K., and J. Trogadis (1984) Computer assisted reconstruction from serial electron micrographs: A tool for systematic study of neuronal form and function. *Annu. Rev. Neurobiol.* 5:341-369.
- Van Harreveld, A., and E. Fikova (1975) Swelling of dendritic spines in the fascia dentata after stimulation of the perforant fibers as a mechanism of post-tetanic potentiation. *Exp. Neurol.* 49:736-749.
- Wenzel, J., C. Schmidt, G. Duwe, W.G. Skrebitz, and I. Kudrjats (1985) Stimulation-induced changes of the ultrastructure of synapses in hippocampus following posttetanic potentiation. *J. Hirnfor.* 26(5):573-583.
- Wilson, C.J. (1984) Passive cable properties of dendritic spines and spiny neurons. *J. Neurosci.* 4:281-297.
- Wilson, C.J., P.M. Goves, S.T. Kitai, and J.C. Linder (1983) Three dimensional structure of dendritic spines in rat striatum. *J. Neurosci.* 3:383-398.